Clim Dyn (2016) 47:2935–2953
DOI 10.1007/s00382-016-3006-x

Projections of glacier change in the Altai Mountains under twenty-first century climate scenarios

Yong Zhang[1] · Hiroyuki Enomoto[1,2] · Tetsuo Ohata[1] · Hideyuki Kitabata[3] · Tsutomu Kadota[3] · Yukiko Hirabayashi[4]

Received: 7 October 2015 / Accepted: 21 January 2016 / Published online: 30 January 2016

Abstract We project glacier surface mass balances of the Altai Mountains over the period 2006–2100 for the representative concentration pathway (RCP) 4.5 and RCP8.5 scenarios using daily near-surface air temperature and precipitation from 12 global climate models in combination with a surface mass balance model. The results indicate that the Altai glaciers will undergo sustained mass loss throughout the 21st for both RCPs and reveal the future fate of glaciers of different sizes. By 2100, glacier area in the region will shrink by 26 ± 10 % for RCP4.5, while it will shrink by 60 ± 15 % for RCP8.5. According to our simulations, most disappearing glaciers are located in the western part of the Altai Mountains. For RCP4.5, all glaciers disappearing in the twenty-first century have a present-day size smaller than 5.0 km^2, while for RCP8.5, an additional ~7 % of glaciers in the initial size class of 5.0–10.0 km^2 also vanish. We project different trends in the total meltwater discharge of the region for the two RCPs, which does not peak before 2100, with important consequences for regional water availability, particular for the semi-arid and arid regions. This further highlights the potential implications of change in the Altai glaciers on regional hydrology and environment.

✉ Yong Zhang
zhangy@lzb.ac.cn

1 Arctic Environment Research Center, National Institute of Polar Research, Tokyo 190-8518, Japan

2 The Graduate University for Advanced Studies, Tokyo 190-8518, Japan

3 Japan Agency for Marin-Earth Science and Technology, Yokohama 237-0061, Japan

4 Institute of Engineering Innovation, The University of Tokyo, Tokyo 113-8656, Japan

Keywords Glacier mass balance · Climate change · GCM · Water availability · Altai glaciers

1 Introduction

Mountain glaciers around the world are retreating and losing mass, which has direct implications for sea level, water resources and natural hazards (Vaughan et al. 2013). Like most mountain glaciers, those in the Altai Mountains have generally retreated during the past few decades with notably accelerated mass loss in recent years (Surazakov et al. 2007; Shahgedanova et al. 2010; Kadota et al. 2011; Narozhniy and Zemtsov 2011; Yao et al. 2012; Wei et al. 2015). The glaciers in this region are an important source of fresh water for the upper tributaries of the Ob and Yenisei rivers (Wang and Cho 1997; Shi et al. 2005; Dyurgerov et al. 2010). Meltwater from the Chinese Altai glaciers contributes ~7.7 % of the total river runoff in the Irtysh River basin (the largest tributary of the Ob River) (Shi et al. 2005; Li et al. 2010), and the glaciers in Mongolia provide ~10.8 % of the total water resources (Pan 2013). Furthermore, mass losses of these glaciers have contributed to sea-level change over the past few decades (Dyurgerov 2010; Radić and Hock 2011; Marzeion et al. 2012). Consequently, glacier wastage in this region has had a major impact on matters ranging from regional water availability and hydrology to global sea-level change. In a warmer future climate (Collins et al. 2013), retreat and thinning of these glaciers are expected to accelerate, leading to an increase in the severity of these concerns.

Although recent glacier changes and climatic trends in the Altai Mountains have been reported (Kalugin et al. 2007; Narozhniy and Zemtsov 2011; Wei et al. 2015), no study has specifically addressed the future surface mass balance and fate of glaciers of different sizes in the region. This is mainly because of a scarcity of observations on glaciers for model calibration and validation, as well as difficulties in correction for biases in climate input data in complex mountainous regions. Although many challenges to project the future surface mass balance of the Altai glaciers remain, several new data sets that allow the model to project glacier surface mass balance at the regional scale with less uncertainties have been developed in recent years (e.g. Kitabata et al. 2014; Pfeffer et al. 2014; Sugiura et al. 2014; Nuimura et al. 2015).

In this study, we project the surface mass balance for each elevation band of every glacier in the Altai Mountains from the present to 2100 using a temperature index-based glacier mass balance model. The model considers refreezing of meltwater, feedback between surface mass balance and changing glacier hypsometry, and spatial variability in model parameters. The model is driven by daily near-surface temperature and precipitation projections from 12 general circulation models (GCMs) forced by two representative concentration pathway (RCP) radiation forcing scenarios (Van Vuuren et al. 2011). The GCM outputs are bias-corrected using the Weather Research and Forecasting (WRF) model simulations, with a resolution of 5 km. Our study focuses on the ultimate fate of glaciers of different sizes as revealed by projections of glacier surface mass balance, and analyzes the potential implications of those changes on the Altai Mountains and surrounding areas.

2 Study area and data

2.1 Study area

The Altai Mountains span the westernmost extent of Mongolia and the common border regions of north-western China, eastern Kazakhstan, and Russia (Fig. 1). The region contains 1281 glaciers with a total area of 1191 km^2 (Arendt et al. 2014; Nuimura et al. 2015). The glaciers are located primarily in the Katun and Chuya ridges, the Tavan Bogd, and the Tsambagarav and Kharkhiraa massifs (Fig. 1) and span an elevation range of 1945–4470 m a.s.l., within which nearly 80 % of the glacier area lies between 2800 and 3700 m a.s.l. Among all Altai glaciers, 77.2 % are <1.0 km^2 and contribute 27 % of the total glacier area, and 3.1 % are >5.0 km^2 and contribute 29 % of the total area (Fig. 2a; Table 1). Small glaciers with an area of <1.0 km^2 are predominant in the Katun and Chuya ridges and the Tavan Bogd, where nearly 60 % of the glacier area lies below the elevation of 3000 m a.s.l. (Fig. 3), whereas the majority of Mongolian glaciers have an area >1.0 km^2 and lie above the elevation of 3000 m a.s.l. (Fig. 3). Observations of these glaciers have been limited, but surface mass balance measurements have been collected for six of the glaciers over different periods (WGMS 2014).

The climate of this region is characterized by the westerly circulation in summer and the Siberian High in winter (Panagiotopoulos et al. 2005). Meteorological observations

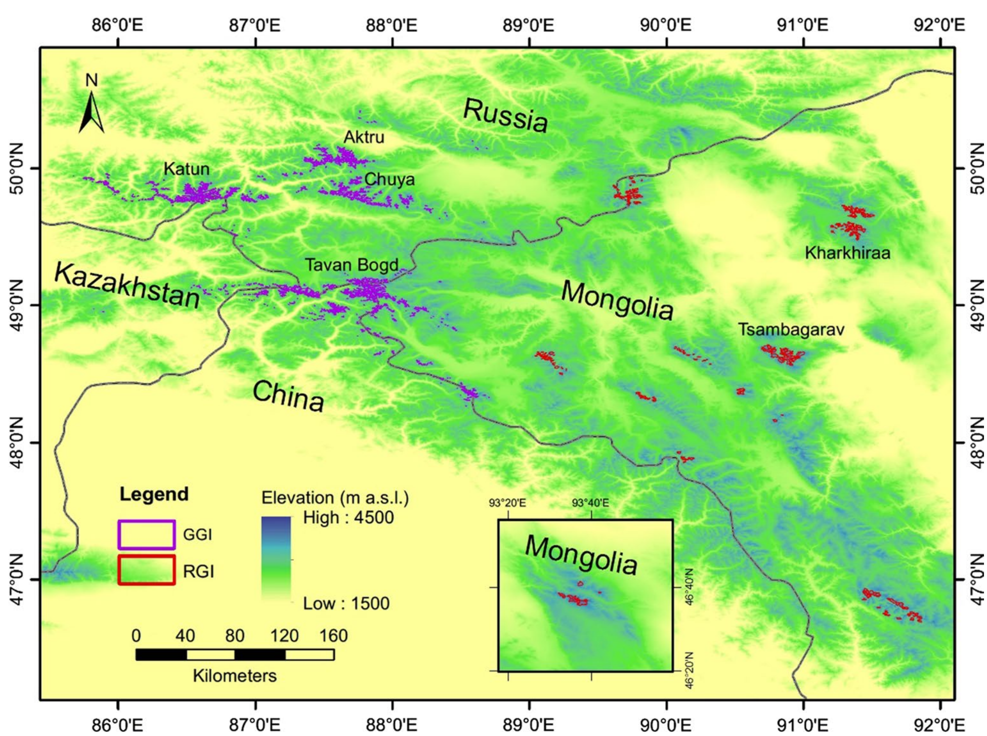

Fig. 1 Glacier distribution in the Altai Mountains. Glacier outlines are from the GGI and the RGI. The *inset* shows the glacier distribution in the south-eastern part of Mongolia. Aktru denotes the Aktru River basin, including the Leviy Aktru, Maliy Aktru, Praviy Aktru, and Vodopadniy glaciers

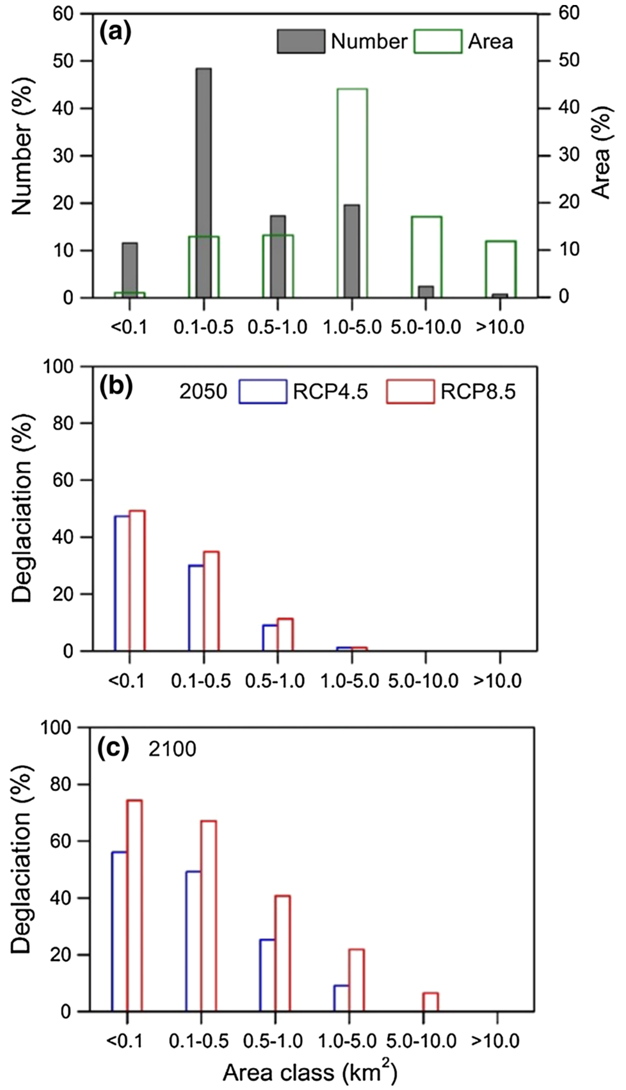

Fig. 2 Present-day glacier distribution in different area size classes (**a**), and projected deglaciation in these area size classes for RCP4.5 and RCP8.5 in 2050 (**b**) and 2100 (**c**)

Table 1 Projected disappearing glacier in different area size classes by the end of the century for RCPs relative to 2005 values

Area class (km^2)	Present number	RCP4.5 (%)	RCP8.5 (%)
<0.1	148	56.0	74.0
0.1–0.5	620	49.0	67.0
0.5–1.0	221	25.0	41.0
1.0–5.0	252	9.0	22.0
5.0–10.0	31	0.0	7.0
>10.0	9	0.0	0.0

indicate that winter precipitation accounts for 10–30 % of annual totals, and the proportion of winter precipitation increases with elevation as the influence of the Siberian High diminishes (Surazakov et al. 2007; Shahgedanova et al. 2010). Increases in air temperature, varying from 0.6 to 1.1 °C for the period of 1952–2005, have been observed in different regions (Surazakov et al. 2007; Shahgedanova et al. 2010; Narozhniy and Zemtsov 2011; Yao et al. 2012).

2.2 Data

2.2.1 *Glacier area, hypsometry and length*

We use two glacier inventories, the Glacier Area Mapping for Discharge from the Asian Mountains (GAMDAM) Glacier Inventory (GGI; Nuimura et al. 2015) and the Randolph Glacier Inventory version 4.0 (RGI; Arendt et al. 2014), to extract the glacier information needed for the model. The RGI is a global collection of digital outlines of the world's glaciers, excluding the Greenland and Antarctic ice sheets (Pfeffer et al. 2014). However, explicit glacier outlines are missing in the RGI4.0 for many areas of the western part of the Altai Mountains, and these glaciers are represented as circles (Pfeffer et al. 2014). Therefore, the GGI, a new glacier inventory for high-mountain Asia (Nuimura et al. 2015), is used for the glaciers of the western part of the region (Fig. 1). In total, 1281 glaciers with an area of 1191 km^2 are selected from the two glacier inventories: 249 glaciers located in the eastern part of the region are from the RGI4.0 and the remaining glaciers are from the GGI.

To obtain elevation data for the glaciers that lack elevation information, glacier outlines are draped over the recently released Advanced Spaceborne Thermal Emission and Reflection Radiometer (ASTER) Global Digital Elevation Model Version 2.0 (GDEM2; Tachikawa et al. 2011) and are separated into individual glaciers. Then we can obtain the mean, maximum and minimum elevation data from the ASTER GDEM2. For the glaciers recorded in the GGI, glacier length is calculated based on a relation between glacier length and maximum and minimum elevations (Hirabayashi et al. 2013).

2.2.2 *Glacier mass balance*

In situ measurements of surface mass balance are available for six glaciers over different time periods, and these are obtained from the World Glacier Monitoring Service (WGMS 2014). Due to the different periods of measurement and simulation, the observations on four glaciers can be used to evaluate the model performance. These glaciers are the Leviy Aktru, Maliy Aktru, Praviy Aktru, and Vodopadniy glaciers (Table 2), which are located in the Aktru River basin (Fig. 1). The time series of surface mass balance of the Aktru River basin over the period 1977–2005

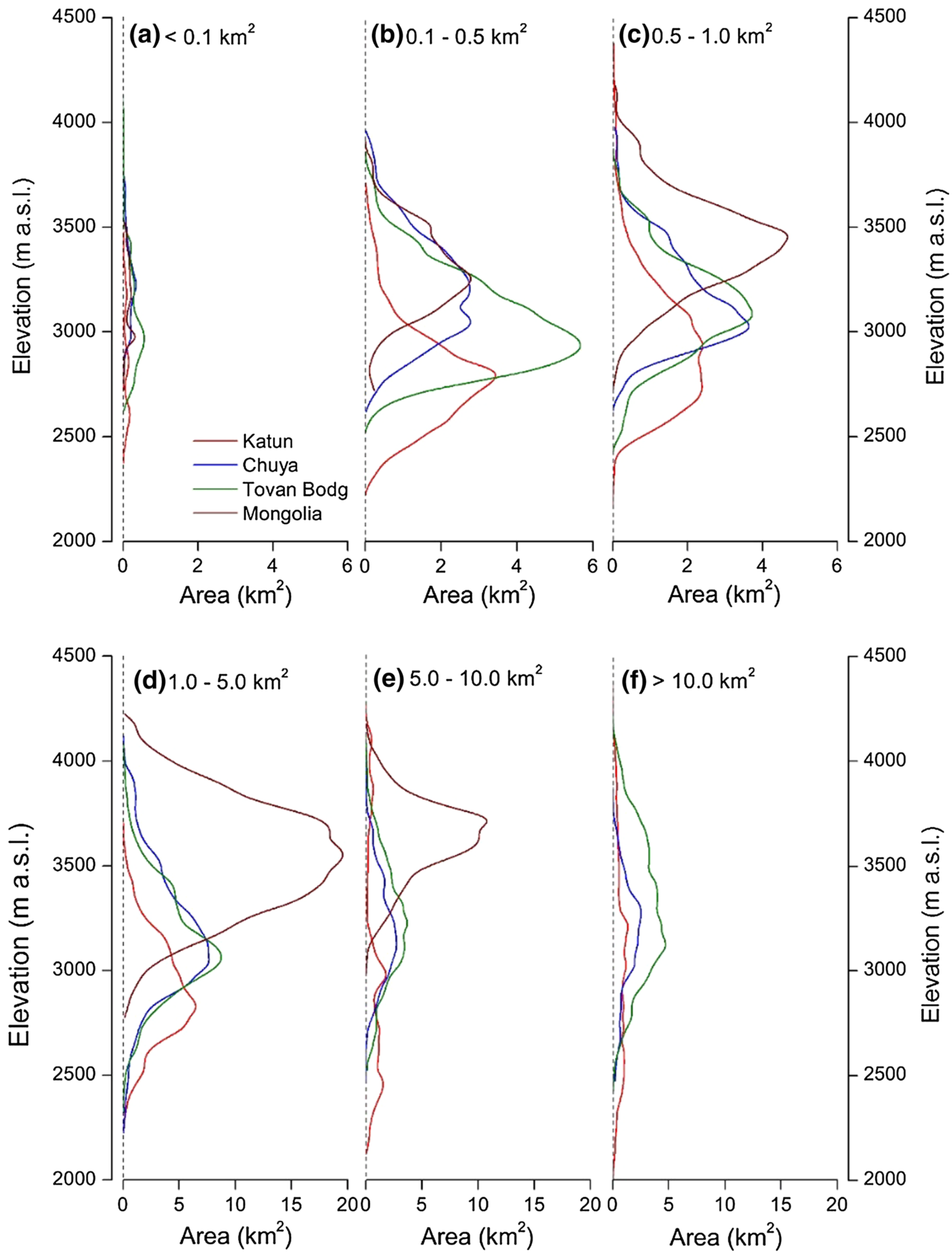

Fig. 3 Area-altitude distribution of present-day glaciers of different area size classes in different regions of the Altai Mountains

averaged from the observations on the four glaciers is also used for model validation.

Moreover, geodetic mass changes of the 14 glaciers in the Chinese Altai (Table 2), which were estimated based on the Shuttle Radar Topography Mission Digital Elevation Model and the ASTER images (Wei et al. 2015), are used to validate the model performance.

2.2.3 Climate data

To analyze future changes in the variability of glacier mass balance under climate change conditions, daily near-surface air temperature and precipitation from the 12 GCMs (Table 3) participating in the fifth phase of the Coupled Model Intercomparison Project (CMIP5; Taylor et al. 2012) are used for the projections of the surface mass balances of the Altai glaciers. We employ two GCM simulations, including historical simulations (1950–2005) forced by natural (e.g. volcanic and solar) and anthropogenic (e.g. greenhouse gases and ozone) forcings and future simulations (2006–2100) forced by the RCP scenarios (Van Vuuren et al. 2011). The RCPs span a range of radiative forcing values from 2.6 to 8.5 W m^{-2}, where the values indicate the increase in radiative forcing by the end of the

Table 2 Characteristics of observed glaciers in the Altai Mountains

Glacier	Region	Elevation (m a.s.l.)	Area (km^2)	Observed period
Leviy Aktru (LA)	Aktru basin	2665–4030	5.95	1977–2011
Maliy Aktru (MA)	Aktru basin	2267–3710	2.73	1962–2011
Praviy Aktru (PA)	Aktru basin	2445–3668	3.88	1980–1990
Vodopadniy (VP)	Aktru basin	2716–3549	0.98	1977–2011
W01	Chinese Altai	2432–4362	26.75	1999–2008
W02	Chinese Altai	2597–3700	8.79	1999–2008
W03	Chinese Altai	2728–3987	6.55	1999–2008
W04	Chinese Altai	2266–3780	4.55	1999–2008
W05	Chinese Altai	2504–3763	3.70	1999–2008
W06	Chinese Altai	2514–3770	3.01	1999–2008
W07	Chinese Altai	2718–3696	4.62	1999–2008
W08	Chinese Altai	2462–3837	3.06	1999–2008
W09	Chinese Altai	2499–3202	1.74	1999–2008
W10	Chinese Altai	2658–3559	3.59	1999–2008
W11	Chinese Altai	2660–3619	2.05	1999–2008
W12	Chinese Altai	2820–3480	2.39	1999–2008
W13	Chinese Altai	2622–3389	2.84	1999–2008
W14	Chinese Altai	2576–3308	3.73	1999–2008

Area and elevation range of the four glaciers in the Aktru River basin are from the GGI, and the fourteen glaciers in the Chinese Altai are from Wei et al. (2015)

Table 3 Summary of the 12 CMIP5 GCMs selected for this study

Model	Institute	No. of grids
CCCma-CanESM2	Canadian Centre for Climate Modelling and Analysis, Canada	128 × 64
CMCC-CM	Centro Euro-Mediterraneo per I Cambiamenti Climatici, Italy	480 × 240
CNRM-CM5	Centre National de Recherches Meteorologiques/Centre Europeen de Recherche et Formation Avancees en Calcul Scientifique, France	256 × 128
CSIRO-Mk3.6.0	Commonwealth Scientific and Industrial Research Organization in collaboration with the Queensland Climate Change Centre of Excellence, Australia	192 × 96
GFDL-ESM2G	Geophysical Fluid Dynamics Laboratory, USA	144 × 90
INM-CM4	Institute for Numerical Mathematics, Russia	180 × 120
IPSL-CM5A-LR	Institute Pierre-Simon Laplace	96 × 96
MIROC5	Atmosphere and Ocean Research Institute, National Institute for Environmental Studies, and Japan Agency for Marine-Earth Science and Technology, Japan	256 × 128
MPI-ESM-LR	Max Planck Institute for Meteorology (MPI-M), Germany	192 × 96
MRI-CGCM3	Meteorological Research Institute, Japan	320 × 160
NCAR-CCSM4	National Center for Atmospheric Research, USA	288 × 192
NCC-NorESM1-M	Norwegian Climate Centre, Norway	144 × 96

The institution and model names are taken from http://cmip-pcmdi.llnl.gov/cmip5/availability.html. Size information is extracted from data headers

twenty-first century relative to pre-industrial values, and represent various possible climate outcomes (Moss et al. 2010). Here, we use the results for the moderate RCP4.5 and the most extreme RCP8.5 scenarios.

To bias-correct the GCM outputs, we use daily data sets of near-surface air temperature and precipitation simulated by the Advanced Research version of the Weather Research and Forecasting (WRF) model (Skamarock et al. 2008). The WRF, a fully compressible and nonhydrostatic model (Skamarock and Klemp 2008; Skamarock et al. 2008), was applied to a domain of 1000 km × 1000 km covering the Altai Mountains with 45 vertical levels (Kitabata et al. 2014; Sugiura et al. 2014). WRF outputs are available for the period 1988–2011 at a spatial resolution of 5 km. A detailed description of the WRF can be found in Skamarock et al. (2008). Daily air temperature, accumulated precipitation amount and snow water equivalent (SWE) in the Altai Mountains simulated by the WRF were validated by comparison with the Global Surface Summary of the Day product from the National Climate Data Center of the National Oceanic and Atmospheric Administration (NOAA), local observations of summer precipitation in 2006, and snow surveys from the Mongolian Altai Mountains in 2008 (Kitabata et al. 2014; Sugiura et al. 2014). The comparisons confirmed that the surface temperature, precipitation, and SWE were simulated accurately using the WRF, especially for high-elevation regions. In particular, the WRF well simulated the elevation dependency and seasonality of precipitation and SWE in the presence of spatial variability (Kitabata et al. 2014; Sugiura et al. 2014).

3 Methods

3.1 Meteorological data pre-processing

Each glacier of this region is divided, at intervals of 50 m, into a set of elevation bands. The area of each elevation band is determined using a normal distribution derived from glacier area and the range between maximum and minimum elevation. For each elevation band of the glacier, the air temperature and precipitation time series are interpolated according to its mean elevation using altitude-dependent lapse rates. As shown by previous studies (Surazakov et al. 2007; Shahgedanova et al. 2010; Kitabata et al. 2014), air temperature decreases with increasing altitude with a constant lapse rate, whereas precipitation increases with altitude with a precipitation gradient. Due to the lack of observed meteorological and glaciological data sets in high-elevation glacierized regions, little is known about the spatial variability of the temperature lapse rate or the precipitation vertical gradient. In this study, these parameters are not spatially uniform in the model, and their spatial variability is considered when air temperature and precipitation time series are generated for each elevation band. These parameters are estimated at each glacier location by regressing the temperature and precipitation of 4×4 WRF grid points around the glacier onto elevation, longitude, and latitude. Previous studies have confirmed that this approach is reasonable and useful for temperature and precipitation estimations at unsampled sites (e.g. Fang and Yoda 1988; Marzeion et al. 2012; Li et al. 2013).

3.2 Glacier mass-balance model

A temperature index-based glacier mass balance model is used to calculate surface mass balance for each of the Altai glaciers, which is based on the model developed by Hirabayashi et al. (2010, 2013). The main components of the model are identical to those in Hirabayashi et al. (2010, 2013). Thus, the model is described only briefly here before highlighting the modifications that we made. The model computes the major components of the glacier mass budget. The surface mass balance is calculated for each 50 m elevation band of each individual glacier with daily resolution. The mass-balance year is from 1 October to 30 September of the following year.

Snow and ice melt is calculated for each elevation band through a temperature-index model that is based on an empirical relationship between melt and air temperature (Braithwaite and Zhang 2000; Hock 2003). Degree-day factors (DDFs) in the model are different for snow and ice, and ice melting in an elevation band occurs only if no snowpack remains in the band. Surface accumulation for each elevation band is modelled from the precipitation value using a temperature threshold of 2 °C to differentiate snow from rain. At or below that temperature, snow is considered to fall. A mixture of snow and rain is assumed within a transition zone ranging from 1 K above to 1 K below the threshold temperature. Within this temperature range, the snow and rain percentages of total precipitation are obtained by linear interpolation. The dynamic response of each glacier to surface mass change is simulated by applying volume-area and -length scaling, which is based on a theoretical analysis of glacier dynamics and glacier geometry (Bahr 1997; Bahr et al. 1997). Volume-area scaling is used to estimate glacier volume from glacier area and to update glacier area after computation of glacier mass balance and thus the volume change after each time step. We use volume-length scaling to adjust glacier length when volume changes. The change in glacier length determines the elevation range of a glacier, which allows for the removal or addition of elevation bands at the terminus (Radić et al. 2008). When a glacier retreats, the area change is computed from the area-altitude distribution of the lost elevation bands, whereas in the case of glacier advance, the length is allowed to increase assuming that the normalized area-altitude distribution is kept unchanged.

For the model of Hirabayashi et al. (2010, 2013), the refreezing process was not taken into account in the mass balance calculation. When melting occurs at the surface of a cold snowpack, some of the surface meltwater can percolate into the snowpack and refreeze, with the consequence that surface melting does not necessarily equate to mass loss for a glacier. In this study, refreezing is estimated for each elevation band based on a relation between the potential depth of meltwater refreezing and the mean annual air temperature (Woodward et al. 1997). Moreover, the previous version of the model aggregated the individual glaciers into one large glacier in each grid cell and then calibrated the DDFs for each grid cell until yielding maximum agreement with the grid cell-specific average of the total glacier mass balance observed at 295 measurement sites (Hirabayashi et al. 2010, 2013). In the Altai Mountains, there are mass balance measurements for six glaciers, four of which are located in the same basin. The undersampling leads to strong limits on the reliability and representativeness of the DDFs. Here, a set of empirical functions, which relates the observed DDFs for snow and ice on 40 glaciers to the climatic setting of each glacier (defined by annual temperature and precipitation from the gridded climate data), the mean glacier elevation, and the geophysical location from the glacier inventory, is used to estimate DDFs for snow and ice. The set of 40 glaciers are distributed in the Tibetan Plateau, Tien Shan, Altai Mountains, and surrounding areas, and most of these are located in a region that has a similar distribution of annual temperature range and a similar ratio of summer precipitation to annual precipitation (>40 %) (Sakai et al. 2015). For these glaciers, DDFs were calculated from observed snow/ice ablation data (e.g. Zhang et al. 2006; Yang et al. 2010; Kadota et al. 2011; Liu et al. 2011; Liu and Liu 2015).

3.3 Bias correction of the GCM data

We spatially interpolate all outputs of the CMIP5 GCMs from the original resolutions (specified in Table 3) to 0.5° × 0.5° using a bilinear interpolation. The bilinear interpolation is preferred to a simple re-gridding method as it provides a realistic spatial gradient rather than patches of same values from a GCM grid in multiple 0.5° grid cells (Koirala et al. 2014). Note that biases in temperature and precipitation are well recognized features of GCM-simulated climate fields, which must be corrected prior to use at the local glacier scale. The delta change approach (Hay et al. 2000; Graham et al. 2007; Sperna Weiland et al. 2010; Clarke et al. 2015) is employed to separate and remove GCM bias while retaining variability. For the bias correction of the GCM outputs, monthly scaling factors are calculated from the difference (temperature) or ratio (precipitation) in 18-year average monthly means between the WRF time series and the GCM time series for the period 1988–2005. For temperature and precipitation an additive correction and a multiplicative correction are used, respectively, as

$$T_{corrected} = T_{GCM} + (\bar{T}_{WRF} - \bar{T}_{GCM}), \quad (1)$$

$$P_{corrected} = P_{GCM} \times (\bar{P}_{WRF} / \bar{P}_{GCM}), \quad (2)$$

where T and P are the daily temperature and precipitation, $\bar{T}$ and $\bar{P}$ are the 18-year average monthly temperature and precipitation, and subscripts '*WRF*', '*GCM*', and '*corrected*' denote WRF, GCM, and bias-corrected data. Applying the monthly correction factors also implies downscaling the GCM data spatially to the higher spatial resolution of the WRF dataset, because correction factors are calculated for all individual cells of the WRF grid.

Applying the approach as indicated in Eq. (2) may result in unrealistic precipitation peaks in the bias-corrected precipitation time series due to large differences between the bias-corrected and observed amount and the number of wet days for some regions. Therefore, the bias-correction of precipitation, Eq. (2), is extended with a threshold that has to be exceeded by the total monthly precipitation amount of the GCM before the multiplicative correction can be used (Van Beek 2008; Sperna Weiland et al. 2010; Zhang et al. 2015). The threshold ($\bar{P}_{WRF} / \bar{N}_{WRF}$) equals the mean daily precipitation amount for the present month according to the WRF data, which is defined as the 18-year average monthly precipitation divided by the 18-year average number of wet days for the specific month from the WRF data. When the total monthly precipitation of the GCM does not exceed the threshold or the multiplicative correction factor ($\bar{P}_{WRF} / \bar{P}_{GCM}$) exceeds it, the days in which precipitation occurs are calculated from a temperature limit below which a day becomes wet. Applying this approach increases the number of wet days to avoid large rain events on the few days with rain in the GCM time series (Sperna Weiland et al. 2010). The temperature limit (T_{crit}) is estimated as (Van Beek 2008; Sperna Weiland et al. 2010)

$$T_{crit} = T_{\mathrm{min}GCM} + (T_{\mathrm{max}GCM} - T_{\mathrm{min}GCM}) \frac{\bar{N}_{WRF}}{N}, \quad (3)$$

where T_{max} and T_{min} are the maximum and minimum temperature of the given month, and N is the total number of days in the specific month. Consequently, the number of wet days of the GCM per month (N_{GCM}) is estimated, and the corresponding daily amount of precipitation for these days ($P_{corrected\_w}$) is estimated as

$$P_{corrected\_w} = \bar{P}_{WRF} / N_{GCM}, \quad (4)$$

3.4 Model validation

Our modelling approach is validated through a multilayer procedure including all available observed or previously estimated data sets for the study region. These data include: (1) observed annual mass balances for the four glaciers (Leviy Aktru, Maliy Aktru, Praviy Aktru and Vodopadniy glaciers); (2) geodetic mass changes of the fourteen glaciers in the Chinese Altai (Wei et al. 2015); and (3) changes in glacier area in the Aktru River basin and Chinese Altai, estimated from satellite data (Narozhniy and Zemtsov 2011; Wei et al. 2015) and from WRF meteorological data (Zhang et al. 2014).

Two assessment criteria are used to evaluate the performance of the model, the correlation coefficient (r) and the mean absolute error (MAE). The MAE is preferred to the commonly used root mean square error (RMSE) because it provides a more robust indicator of the sizes of typical errors. MAE is defined as

$$MAE = \frac{1}{n}\sum_{i=1}^{n}\left|B_{obs,i} - B_{\mathrm{mod},i}\right| \tag{5}$$

in which n is the number of observations, B is the specific mass balance, and subscripts 'obs' and 'mod' denote observed and modelled data.

4 Results

4.1 Model validation

According to our estimations, the temperature lapse rates vary from −0.45 °C (100 m)$^{-1}$ to −0.90 °C (100 m)$^{-1}$ with an average value of −0.70 °C (100 m)$^{-1}$, whereas the precipitation vertical gradients vary from 1.1 % (100 m)$^{-1}$ to 15.0 % (100 m)$^{-1}$ with an average value of 9.0 % (100 m)$^{-1}$. Our estimated average temperature lapse rate is slightly less than that used in the Altai by Radić and Hock (2011; −0.81 °C (100 m)$^{-1}$), and the average precipitation gradient is slightly larger than that given by Radić and Hock (2011; 8.0 % (100 m)$^{-1}$). Similarly, the DDFs for ice vary from 6.0 to 11.0 mm day^{-1} °C^{-1} with an average value of 8.6 mm day^{-1} °C^{-1}, and those for snow vary from 1.5 to 6.1 mm day^{-1} °C^{-1} with an average value of 4.1 mm day^{-1} °C^{-1}. Our estimated DDFs are similar to those reported in previous studies (Hock 2003; Zhang et al. 2006; Radić and Hock 2011).

To validate our modelling approach, we use observed annual surface mass balance data from the four glaciers over different periods. For each of these four glaciers, we calculate the surface mass balance over the corresponding observation period using bias-corrected GCM outputs and estimated model parameters. We gain, in total, a set of 133 pairs of modelled and observed annual mass balances. A scatter plot of modelled versus observed annual mass balances of the four glaciers is shown in Fig. 4a, which shows a close agreement between the modelled and the observed annual mass balances. The correlation coefficient between the modelled and the observed annual mass balances is 0.77 (significance level $p < 0.001$) and the MAE is 0.21 m w.e. Furthermore, we consider the long-term variation in surface mass balance in Fig. 4b, in which modelled results are consistent with variation in observed annual mass balance in the Aktru River basin over the period 1977–2005.

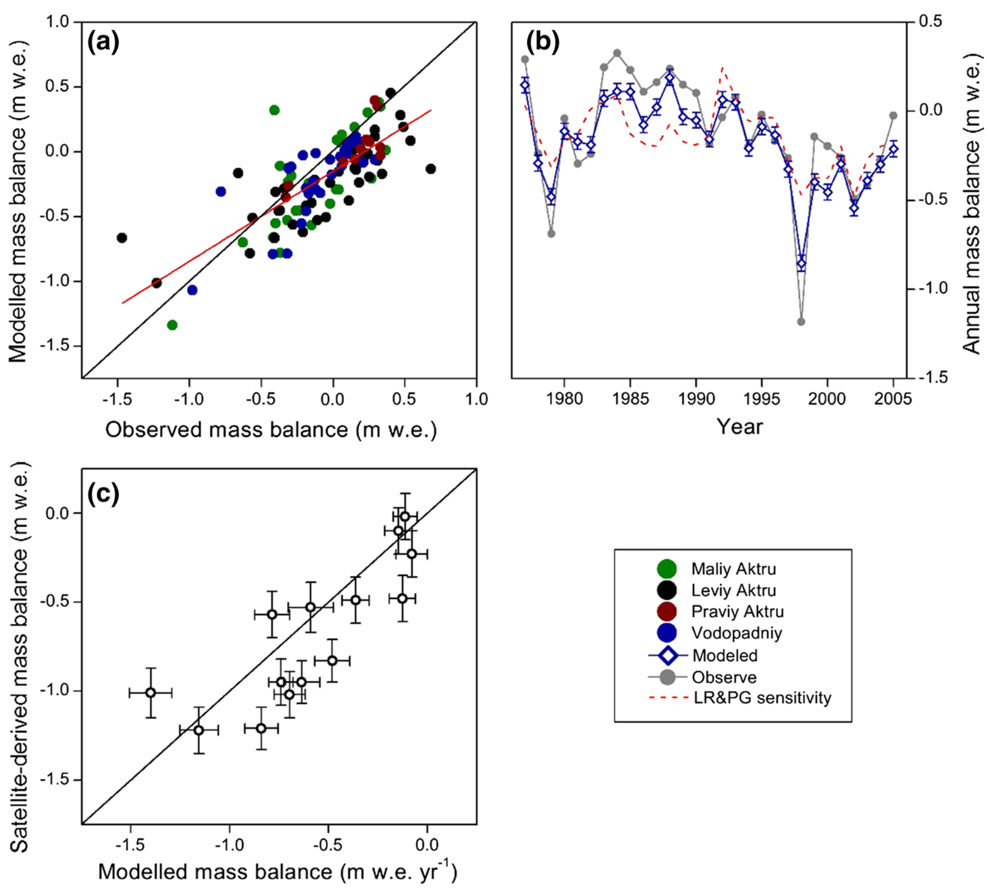

Fig. 4 Scatter diagram of observed versus modelled annual mass balance on different glaciers (**a**), time series of annual mass balances in the Aktru River basin over the period 1977–2005 with a sensitivity of temperature lapse rate (LR) and precipitation gradient (PG) (**b**), and the geodetic mass change rates and the modelled results on fourteen glaciers in the Chinese Altai Mountains (**c**). Satellite-based mass change rates in **c** are from Wei et al. (2015). *Error bars* indicate standard error

The range of modelled mass balances captures the observations well, with a few exceptions (Fig. 4b). In total, the mean modelled mass balance over the period 1977–2005 is –0.16 m w.e., which is slightly more negative than the observation of −0.12 m w.e. in the basin.

Moreover, we calculate the mean surface mass balances over the period 1999–2005 of the 14 glaciers in the Chinese Altai, where mass change rates were estimated using geodetic methods based on satellite data (Wei et al. 2015). A comparison between the modelled results and the geodetic mass change rates of these glaciers is presented in Fig. 4c. We find that the results from the two independent approaches agree well (Fig. 4c), yielding $r = 0.83$ and MAE $= 0.14$ m w.e. year^{-1}. The good agreement with the geodetic approach gives us the confidence to use our model to estimate annual mass changes on individual glaciers over a longer time period.

As an additional analysis of model performance, area change rates of the 4 glaciers in the Aktru River basin and the 14 glaciers in the Chinese Altai were obtained from satellite images for 1999–2008 (Narozhniy and Zemtsov 2011) and 2000–2008 (Wei et al. 2015), respectively. For each of these glaciers, we simulate the area change using bias-corrected GCM outputs for 1999–2005. A comparison of the modelled results and the satellite-based observations is presented in Fig. 5a. For most cases, a satisfying agreement of satellite-derived and calculated glacier area change rate is found ($r = 0.81$ and MAE $= 0.02$ km^2 year^{-1}). The mean change rate in glacier area in these regions is ~0.74 % year^{-1} for the period 1999–2005, slightly less than the satellite-based observation of 0.89 % year^{-1} for the period 1999–2008. This discrepancy may be due mainly to the difference between the simulated and observed periods. Wei et al. (2015) found that an accelerated glacier shrinkage had occurred during the past few decades, especially for the period 1999–2008. We also compare modelled results to those estimated using WRF meteorological data for the same period (Zhang et al. 2014) (Fig. 5b). The modelled results are in good agreement with the previous estimates, yielding $r = 0.83$ and MAE $= 0.01$ km^2 year^{-1}. The mean change rate in glacier area is consistent with the estimate of 0.79 % year^{-1} given by Zhang et al. (2014). This implies that our approach can capture the feedback between glacier mass balance and change in glacier area.

Overall, the modelling approach generally reproduces the observations and the previous estimations well. The good agreement with independent approaches indicates the capability of our modeling approach for simulating variations in surface mass balance and change in glacier area in the study region well. In particular, the bias-corrected GCM outputs are confirmed sufficiently to be used as input for glacier mass balance modelling in the Altai Mountains.

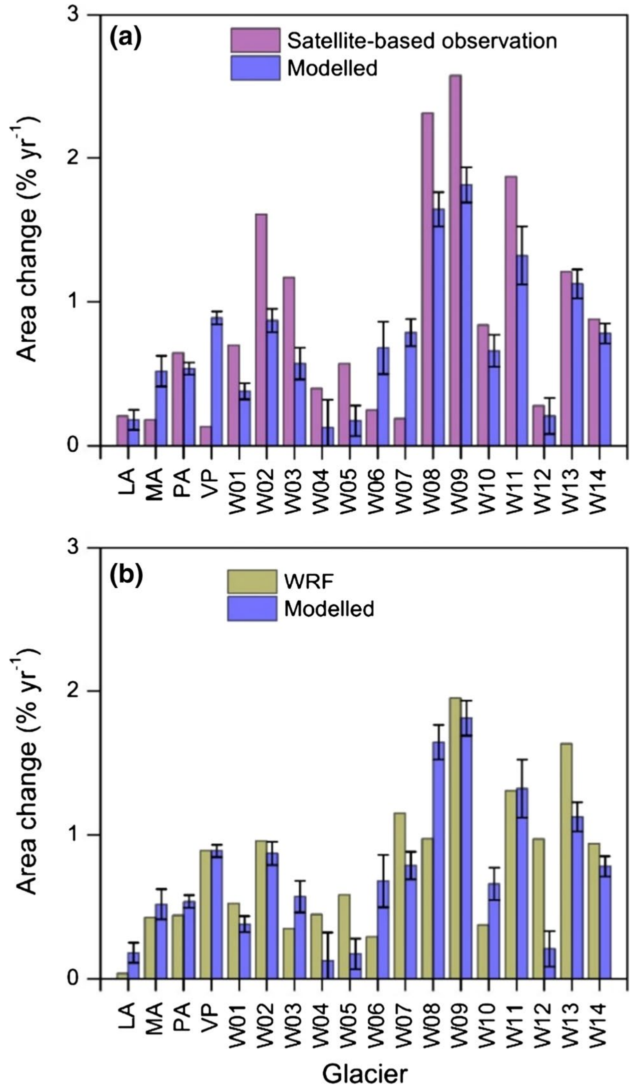

Fig. 5 Satellite-based observed and modelled change rates of glacier area in the Aktru River basin and the Chinese Altai (**a**), and change rates in glacier area estimated using the GCM and WRF outputs over the period 1999–2005 (**b**). Satellite-based observed change rates in glacier area are from Narozhniy and Zemtsov (2011) and Wei et al. (2015), and modelled results using the WRF outputs are from Zhang et al. (2014). *Error bars* indicate standard error. LA, MA, PA, and VP denote the Leviy Aktru, Maliy Aktru, Praviy Aktru, and Vodopadniy glaciers in the Aktru River basin, respectively, and W01–W14 denote the 14 glaciers in the Chinese Altai in Table 2

4.2 Surface mass balance projections

The temperature projections for RCP4.5 and RCP8.5 reveal significant warming in the glacierized region of the Altai Mountains throughout the twenty-first century (Fig. 6a, b), while precipitation is projected to increase slightly with large variability among the GCMs (Fig. 6c, d). The multi-model mean temperature by 2100 is projected to increase at a rate of 0.03 °C year^{-1} for RCP4.5 (Fig. 6a)

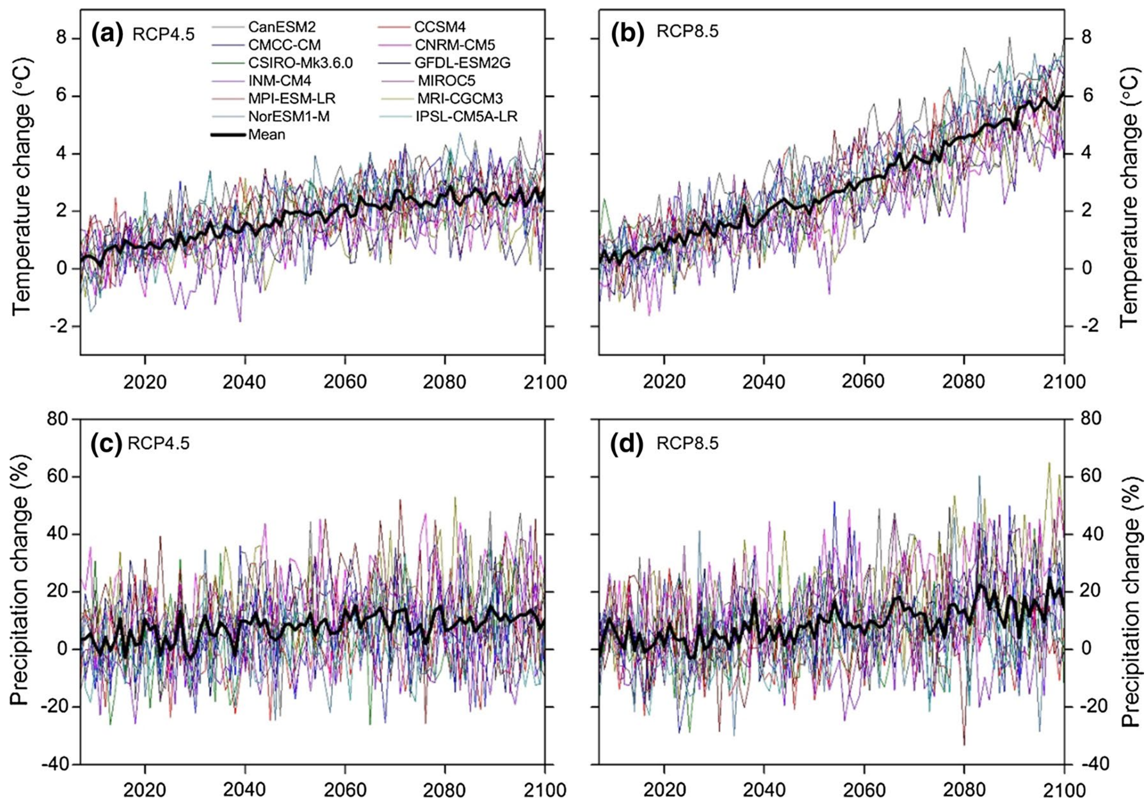

Fig. 6 Projections of changes in temperature and precipitation from 12 GCMs (RCP4.5 *left side*, RCP8.5 *right side*) relative to the 1986–2005 average. *Black curve* in each plot is the mean of the ensemble

and 0.06 °C year^{-1} for RCP8.5 relative to the 1986–2005 average (Fig. 6b). On average, the precipitation by 2100 is projected to increase at a rate of 0.1 % year^{-1} for RCP4.5 and 0.16 % year^{-1} for RCP8.5 relative to the 1986–2005 average. In 2081–2100, the temperature increase exceeds 2.5 °C for RCP4.5 and 5.3 °C for RCP8.5, while precipitation is projected to increase 10.5 % for RCP4.5 and 15.6 % for RCP8.5.

The multi-model means of projected variation in surface mass balances until the year 2100 for RCP4.5 and RCP8.5 are presented in Fig. 7a. In response to increasing temperature, the study region is projected to lose glacier mass continuously throughout the twenty-first century. Over the entire region, the projected mean mass balances are −0.79 and −1.52 m w.e. year^{-1} for RCP4.5 and RCP8.5 during 2006–2100, respectively. The means of the RCP4.5 and RCP8.5 ensembles indicate a trend of stabilization by similar mass loss rates before 2050 (Fig. 7a). Then, the differences between the two RCPs in the rate of mass loss become more obvious towards the end of the century: mass loss remains relatively stable for RCP4.5 but is accelerated for RCP8.5 (Fig. 7a). On average, the annual mass balance of the region is −2.8 m w.e. over the period 2091–2100 for RCP8.5, which is more negative than that for RCP4.5 (−0.6 m w.e.). Before 2050, the temperature rises very rapidly with a rate of 0.04 °C year^{-1} for RCP4.5 and 0.05 °C year^{-1} for RCP8.5 relative to 1986–2005. As a result of increasing temperature, ice melting is projected to be largely enhanced. Although precipitation increases slightly (Fig. 6c, d), the limited change in precipitation is not sufficient to compensate for the increased melting. Aside from the low-altitude zone of the glaciers, enhanced mass loss is found for the entire high-altitude zone (above 3000 m a.s.l.) for the RCPs (Fig. 8), in which the rates of mass loss in 2031–2050 are projected to increase by ~78 % for RCP4.5 and by ~90 % for RCP8.5 relative to 1986–2005, respectively. As a consequence, more mass loss is released from glaciers during this period for both RCPs compared to that in 1986–2005. In the following decades, air temperature continues to increase rapidly for RCP8.5 (Fig. 6b). By 2100, the increase of air temperature for RCP8.5 is about twice as high as that for RCP4.5. Such a sharp rise in air temperature for RCP8.5 leads to continuously accelerated ice melting, which cannot be offset by the limited change in precipitation. Therefore, glacier mass loss continues to increase rapidly for RCP8.5, especially in the high-altitude zone of the glaciers, where the rate of mass loss in 2081–2100 is almost twice as high as that in

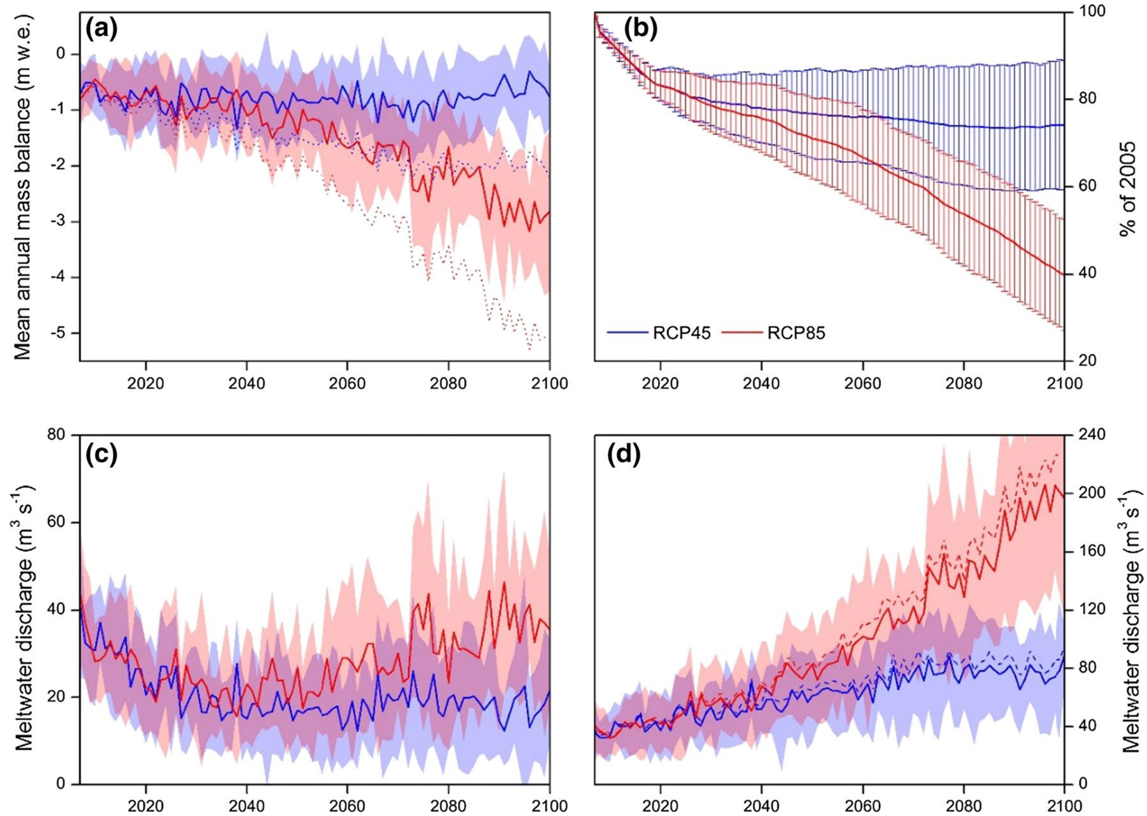

Fig. 7 Projected annual surface mass balance (**a**), changes in glacier area relative to the 2005 ice area (**b**), meltwater discharge (**c**), and meltwater discharge with an assumption of no change in glacier area (**d**) for RCP4.5 and RCP8.5. *Dot line* in **a** indicates surface mass balance with the assumption of no change in glacier area. *Dash line* in d shows meltwater discharge with the assumptions of no change in glacier area and no precipitation change for both RCPs, in which the precipitation is the average value of 1986–2005. *Shading* in **a**, **c** and **d** and *vertical hatching* in **b** denote standard deviation

1986–2005 (Fig. 8b). Compared to the RCP8.5 scenario, a steady increase in air temperature is observed in the second half of this century for RCP4.5, leading to a slight increase in ice melting. Therefore, the ice melting resulting from the increasing temperature can be partly offset by increased precipitation. Compared to 2031–2050, enhanced mass loss is not found in the high-altitude zone (Fig. 8a). In combination with a positive change in precipitation, glacier mass loss for RCP4.5 is not expected to be accelerated and is expected to stabilize by the end of the century.

Figures 9 and 10 show the spatial variability of the surface mass balance for different size glaciers during 2091–2100 for the two RCPs. Significant differences in the mass loss rates are apparent from region to region for the two RCPs. According to our simulations, ~72 % of all Altai glaciers experience mass loss during 2091–2100 for RCP4.5 (Fig. 9). In particular, most of glaciers >1.0 km^2 undergo more significant mass loss compared to those <1.0 km^2 during this period (Fig. 9f). For RCP8.5, ~98 % of these glaciers undergo strong mass loss during 2091–2100 (Fig. 10), especially for glaciers >1.0 km^2 (Fig. 10f). In addition, some areas, such as the eastern parts of the Chuya ridge and the Tavan Bogd, experience slight mass gain for RCP4.5 (Fig. 9), while only 18 glaciers experience slight mass gain for RCP8.5 (Fig. 10).

4.3 Glacier area change

The ensemble of projections for the 12 GCMs shows a substantial decline in glacier area of the region (Fig. 7b). The means of the RCP4.5 and RCP8.5 ensembles show a quick decline in glacier area at similar rates before 2050. As mentioned above, glacier mass loss is accelerated during this period for both RCPs in response to rapid temperature increase, even in the high-altitude zone of the glaciers (Fig. 8). Therefore, enhanced mass loss leads to a rapid reduction in glacier volume and consequent decline in glacier area (Fig. 7b). In particular, small glaciers of <1.0 km^2 contribute almost half of the total reduction of glacier area during this period, while the contribution of glaciers >5.0 km^2 is relatively small (~12 %). A steady change in glacier mass loss results in a slight reduction in glacier volume in the second half of the century for RCP4.5, with the consequence that glacier area declines

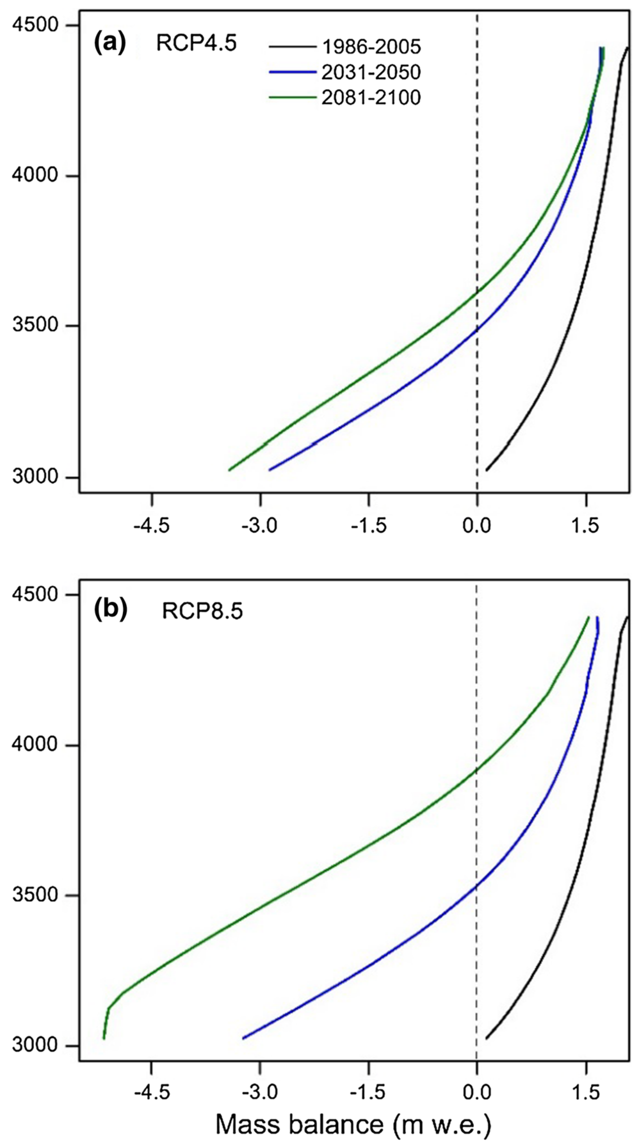

Fig. 8 Projections of surface mass balance in the high-altitude zone of above 3000 m a.s.l. for the periods 1986–2005, 2031–2050, and 2081–2100 for RCP4.5 (**a**) and RCP8.5 (**b**)

steadily. In contrast, an enhanced mass loss leads to a rapid reduction in glacier volume for RCP8.5, for which increased precipitation cannot compensate for increased melt as a result of higher temperature, especially in the high-altitude zone (Fig. 8b). Thus, glacier area continues to decline relatively rapidly for RCP8.5 after 2050 (Fig. 7b). During this period, the contribution of glaciers >5.0 km^2 to the total reduction of glacier area, which is about 23.2 % for RCP8.5, increases largely. In total, the glacier area of the region will decrease by 26 ± 10 % for RCP4.5 and by 60 ± 15 % for RCP8.5 by 2100 (here and throughout, error ranges are for model mean ±σ) relative to the 2005 ice area.

With continued glacier shrinkage, the loss of entire glaciers in the study region begins around 2050 for both RCP scenarios, with widespread ice disappearance by 2100 (Table 4). The two RCP scenarios show a similar trend of ice disappearance by 2050 (Table 4): ~22 % of glaciers disappear with a 5.2 % reduction in ice area for RCP4.5 relative to 2005 values, and ~25 % disappear with a 6.2 % reduction in ice area for RCP8.5. By 2100, ~37 and ~53 % of the Altai glaciers are expected to disappear under RCP4.5 and RCP8.5, respectively, relative to 2005 values, and about 13 and 24 % of the 2005 ice area is expected to be lost.

The majority of the disappearing glaciers are distributed in the Katun and Chuya ridges and the western part of the Tavan Bogd, but a few glaciers in the Mongolian Altai disappear by 2100 (Figs. 9, 10). By the end of the century, all disappearing glaciers are smaller than 5.0 km^2 for RCP4.5 (Fig. 2b). Disappearing glaciers in the size classes of <0.1, 0.1–0.5, 0.5–1.0, and 1.0–5.0 km^2 account for ~56, 49, 25, and 9 % of the total number of the corresponding size class (Table 1), respectively. Compared to the RCP4.5 scenario, more glaciers in each size class will disappear for RCP8.5 (Fig. 2c). Those in the size classes of <0.1, 0.1–0.5, 0.5–1.0, and 1.0–5.0 km^2 account for ~74, 67, 41, and 22 % of the total number of the corresponding size class (Fig. 2c; Table 1), respectively. Notably, ~7 % of glaciers in the size class of 5.0–10.0 km^2 will disappear under RCP8.5 by 2100 (Fig. 2c; Table 1). Most glaciers with an area >5.0 km^2 will survive at the end of the century, but they all experience considerable mass loss and are in a diminished state (Figs. 9, 10), especially for RCP8.5.

4.4 Glacier meltwater projections

The multi-model means of the projected variation in glacier meltwater discharge for RCP4.5 and RCP8.5 are presented in Fig. 7c. The meltwater discharge of the region is projected to decrease initially for both RCPs and then to display different trends in the following decades (Fig. 7c). The means of the RCP4.5 and RCP8.5 ensembles show a decline in meltwater discharge at similar rates before 2050 (Fig. 7c). In the following decades, meltwater discharge decrease slightly and becomes stable for RCP4.5. Relative to the 1986–2005 average, a 39 % decrease in total discharge is projected for 2091–2100 for RCP4.5. In contrast, meltwater discharge is projected to increase for RCP8.5 in the second half of the century, by ~30 % relative to the 1986–2005 average. Furthermore, our multi-model mean indicates that the contribution of glacier loss to sea-level rise for 2006–2100 is projected to be higher than previous estimates for the Altai glaciers (e.g. Dyurgerov 2010; Radić and Hock 2011). The total contribution from the Altai glaciers is ~0.0020 mm year^{-1} for RCP4.5 and ~0.0034 mm year^{-1} for RCP8.5.

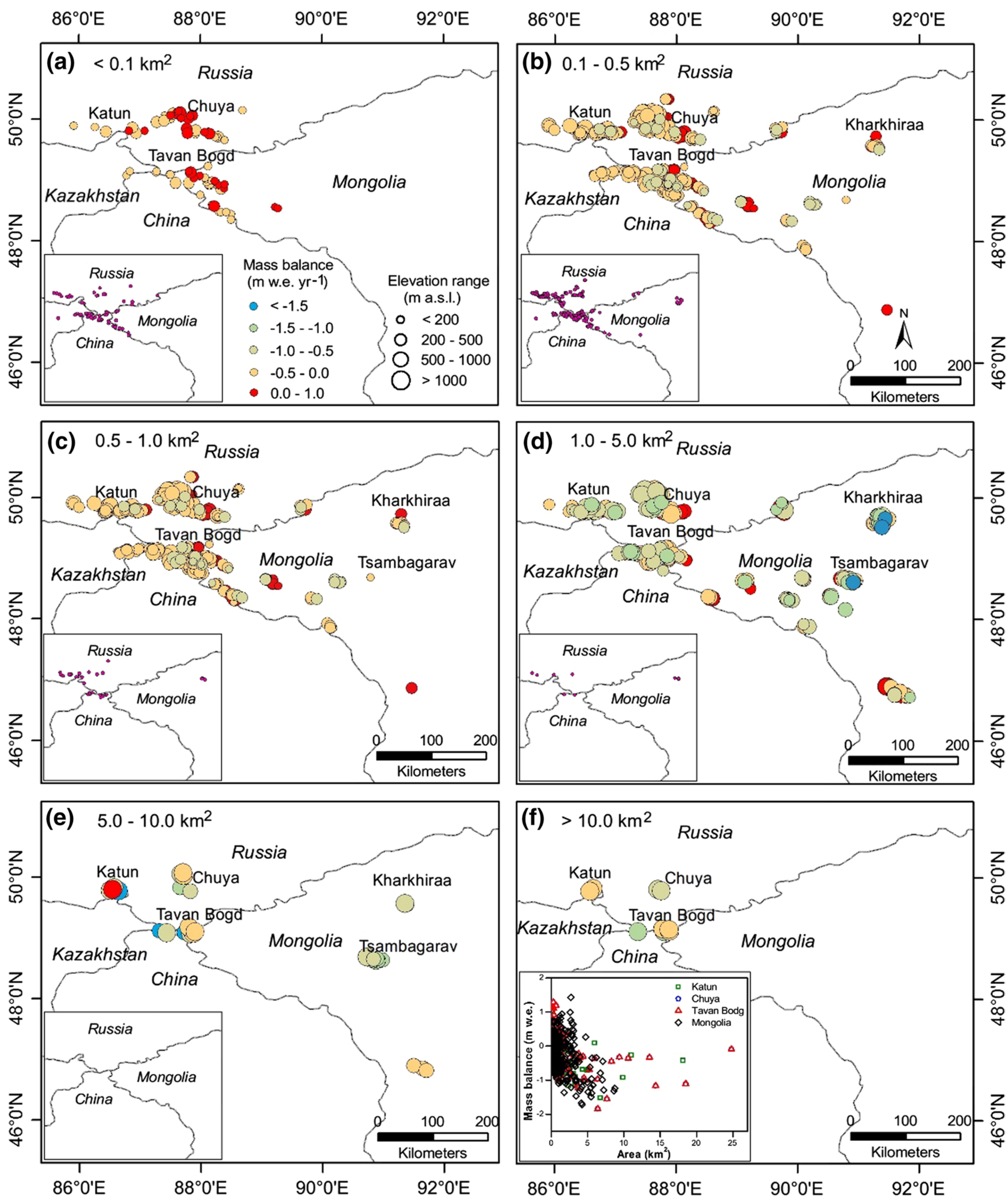

Fig. 9 Spatial variability of projected surface mass balance and disappeared glaciers for different size glaciers during 2091–2100 for the RCP4.5. The *insets* in **a**–**e** indicate spatial distribution of disappeared glaciers for different size glaciers, and scatter plot in **f** shows modelled surface mass balance as a function of glacier area in different regions

5 Discussion

5.1 Fate of the Altai glaciers

Glaciers play an important role in maintaining regional water resources and contributing to global sea-level change, which depends principally on the extent of glacierization in a basin (Casassa et al. 2009; Kaser et al. 2010; Vaughan et al. 2013). This role may be altered significantly by shrinkage of the glacierized area (Jansson et al. 2003; Casassa et al. 2009), especially by glacier disappearance (Clarke et al. 2015; Zhang et al. 2015). Hence, the

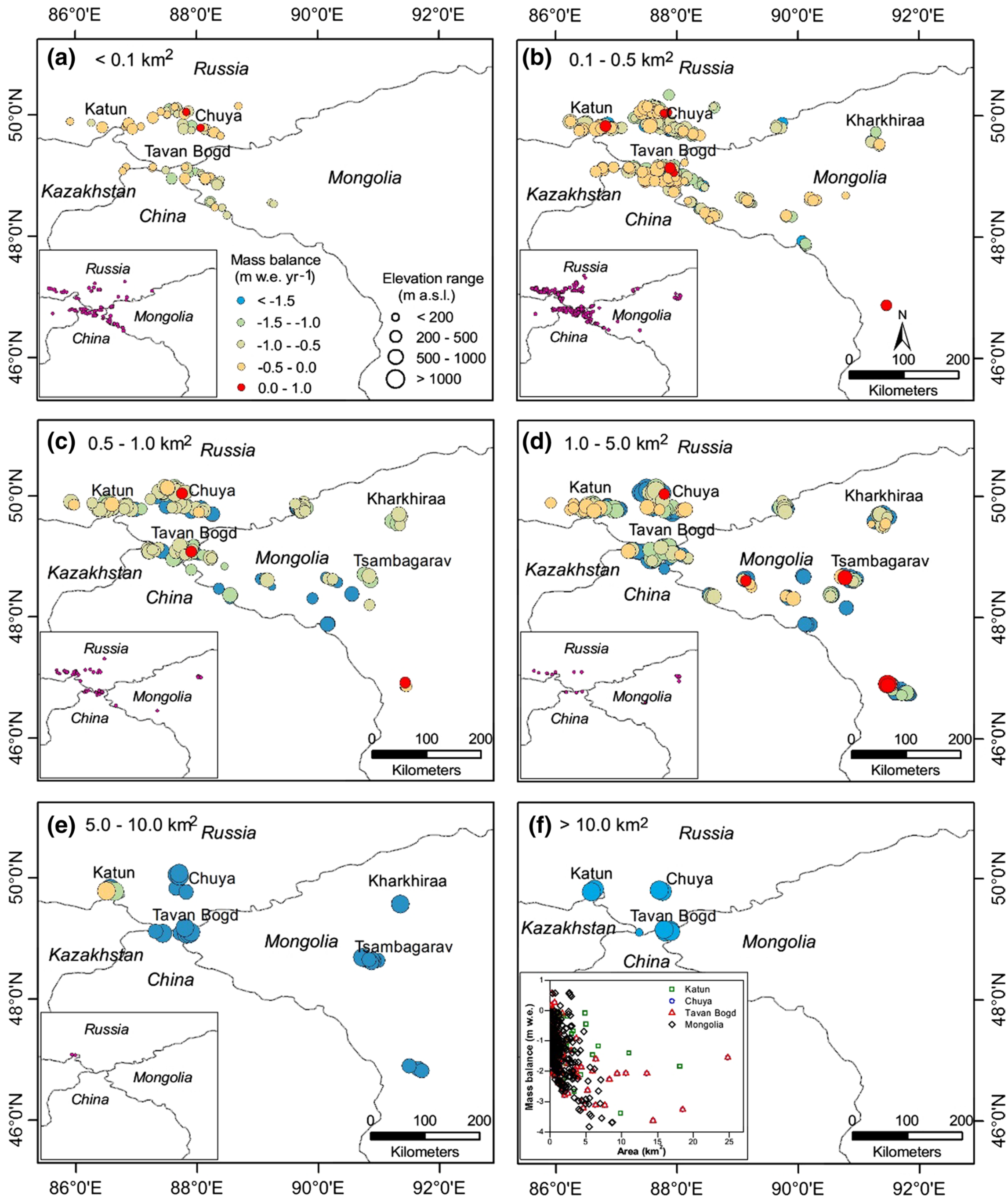

Fig. 10 Spatial variability of projected surface mass balance and disappeared glaciers for different size glaciers during 2091–2100 for the RCP8.5. The *insets* in **a**–**e** indicate spatial distribution of disappeared glaciers for different size glaciers, and *scatter plot* in **f** shows modelled surface mass balance as a function of glacier area in different regions

Table 4 Projected deglaciation in the Altai Mountains for RCPs relative to 2005 values

Year	RCP4.5		RCP8.5	
	Number	Area (%)	Number	Area (%)
2050	278	5.2	467	6.2
2100	467	13.0	673	24.0

future fate of glaciers in a basin has broad implications for regional hydrology and sea-level change.

Our projections in the study region indicate that the fate of these glaciers will vary, depending on their specific characteristics and future climate conditions. Both RCP scenarios indicate that most disappearing glaciers are located in the Katun and Chuya ridges and the western part of the Tavan

Bogd (Figs. 9, 10). The glaciers in these regions are more sensitive to climatic change than those in other parts of the study region (Zhang et al. 2014) because the western part of the region is much wetter than the eastern part (Klinge et al. 2003). Note that glaciers in wetter climate conditions are more sensitive to climate change than those in drier climate conditions (Oerlemans and Fortuin 1992; Braithwaite et al. 2002). An experiment on the climate sensitivity of the Altai glaciers involving changes in precipitation as well as temperature was carried out (Radić and Hock 2011). According to their result, a 10 % increase in precipitation can offset a ~14.3 % increased melt resulting from a 1 K rise in temperature. The ensemble means for both RCPs reveal a significant warming in the study region by 2100 with a limited increase in precipitation (Fig. 6). The warming rate in the western part of the region is slightly higher than that in the eastern part. By the end of this century, the temperature increase for RCP8.5 is twice as high as that for RCP4.5, while precipitation shows a similar trend of increase. Therefore, increased precipitation cannot compensate for enhanced glacier melt due to the rapid warming for RCP8.5, but it may partly offset the melt resulting from the stable change in temperature for RCP4.5. Such effects are evident in the high-altitude zone of the glaciers (Fig. 8). With increased glacier mass loss, glacier volume continues to decrease for the RCPs, especially for small glaciers. As shown in Fig. 3, small glaciers with an area <1.0 km^2 are dominate in these regions, and their area accounts for 77 % of the total area of glacier <1.0 km^2. In particular, nearly 60 % of the glacier area lies below the elevation of 3000 m a.s.l. (Fig. 3). Among all disappearing glaciers, this glacier type accounts for ~95 and ~92 % of these glaciers for RCP4.5 and RCP8.5, respectively. Note that it takes several decades for a glacier to adjust its extent to a change in climate, and the time required for the adjustment increases with glacier size (Bahr et al. 1998; Cuffey and Paterson 2010). The small glaciers therefore will respond more quickly to climate warming by adjusting their extent faster, and thus shrink further. Ultimately, the small glaciers will disappear gradually after losing their volume. The main difference between the RCP4.5 and the RCP8.5 scenarios is the magnitude of temperature rise (Fig. 6), which results in greater mass loss and greater glacier disappearance for RCP8.5 (Fig. 10).

In contrast, glaciers in the Mongolian Altai show the lowest sensitivity to climatic change of any glaciers in the study region (Zhang et al. 2014). Furthermore, most of these glaciers have an area >1.0 km^2 and their elevations are relatively high (Fig. 3). Compared to smaller glaciers, these glaciers will also continue to shrink, but will take more time to respond to climate warming by adjusting their extent. Consequently, most glaciers in the Mongolian Altai are projected to survive by 2100 for the RCPs, but in a diminished state (Figs. 9, 10).

5.2 Peak water

Glacier meltwater is an important contributor to, and modulator of river runoff. It will peak at a certain time, the timing of which is crucial to the future water supply in glacier-affected regions (Jansson et al. 2003; Casassa et al. 2009). The meltwater peak, on a global scale, will occur around 2075 (Radić and Hock 2011), but the timing of the meltwater peak apparently differs from region to region (Casassa et al. 2009; Bliss et al. 2014; Clarke et al. 2015; Zhang et al. 2015). The glaciers in the Altai Mountains are crucial sources of water for the upper tributaries of the Ob and Yenisei rivers (Wang and Cho 1997; Shi et al. 2005; Dyurgerov et al. 2010; Li et al. 2010), especially for the semi-arid and arid regions (Li et al. 2010; Pan 2013). Hence, the hydrologic implications of the projected glacier mass losses are substantial for the study region.

Meltwater discharge in the region is projected to decrease initially for the RCPs and then to display different trends in the following decades (Fig. 7c). Before 2050, glacier shrinkage of the region is accelerated for both RCPs (Fig. 7b). Aside from glaciers disappearing (Table 4), the projected decreases in glacier area for the size classes of <0.1, 0.1–0.5, 0.5–1.0, 1.0–5.0, and 5.0–10.0 km^2 account for ~50, 46, 32, 21, and 13 % of the total area of the corresponding size class for RCP4.5, respectively, while they account for ~53, 51, 36, 24, and 15 % for RCP8.5. To assess the influence of the change in glacier area on the total meltwater discharge of the region, we recalculate the projections of glacier mass balance and meltwater discharge for both RCPs with an assumption of no change in glacier area (Fig. 7a, d). Our recalculations for both RCPs clearly show a continued increase in mass loss and meltwater discharge for the two RCPs before 2050 (Fig. 7a, d). Then, glacier mass loss and meltwater discharge increases quite rapidly for RCP8.5, and increases steadily for RCP4.5 (Fig. 7a, d). Compared to the case with no change in glacier area, we find that increased melting resulting from rapid temperature rise cannot compensate for the dramatic reduction in glacier area for both RCPs before mid-century, leading to a decrease in the total meltwater discharge of the region (Fig. 7c). In the following decades, most of glaciers <1.0 km^2 disappear for the two RCPs (Fig. 2b, c). Mass loss from the surviving glaciers <1.0 km^2 is relatively small for the two RCPs (Figs. 9, 10), particularly for RCP4.5. In contrast, most of glaciers >1.0 km^2 experience significant mass loss during this period (Figs. 9, 10). As a result, meltwater discharge from glaciers <1.0 km^2 contributes only ~18 and 29 % of the total discharge for RCP4.5 and RCP8.5, respectively, and the remaining meltwater is from glaciers >1.0 km^2. In particular, enhanced mass loss is found for the entire high-altitude zone as well as the low-altitude zone of the glaciers for RCP8.5 (Fig. 8b). Even for RCP4.5, a steady increase in air temperature leads to a slight increase in ice melting in the high-altitude zone of the glaciers for RCP4.5 (Fig. 8a). In addition, an experiment involving no change in glacier area as well as precipitation indicates that a limited increase in precipitation can compensate for only ~10 % of increased melting as a result of increasing temperature for the RCPs relative to the case with no change in glacier area (Fig. 7d). It can be seen that although glacier volume continues to decline as a result of continued mass loss, enhanced melting resulting from higher temperature, especially for glaciers >1.0 km^2, can compensate for the reduction of glacier storage with glacier shrinkage for the two RCPs. Consequently, a rapid increase in air temperature leads to significant increase in meltwater discharge in the second half of the century for RCP8.5. On the other hand, a steady increase in air temperature in combination with a positive change in precipitation results in stable variation in meltwater discharge for RCP4.5. These trends are different from those with the assumption of no change in glacier area (Fig. 7c, d).

According to our projections, meltwater discharge in the study region shows different trends by the end of the century for the two RCPs, and the peak is not observed until 2100 (Fig. 7c) despite the persistent negative trend in ice area. However, ~40 % of the 2005 ice area will survive by 2100 for RCP8.5 and most glaciers experience considerable mass losses (Fig. 10). This implies that glacier area is expected to decline continuously in the next century, leading to more meltwater being released from glacier storage. As a consequence, meltwater discharge may peak at a certain time.

5.3 Uncertainties

There are uncertainties in our projections of glacier surface mass balance and associated implications. Here we analyze sources of uncertainties in the projections, which include (1) glacier parameters, (2) orographic effects on precipitation and temperature, and (3) volume-area-length scaling.

Projections of glacier change in the region should consider a very large number of glaciers, each with a different geometry and characteristics. A complete glacier inventory is therefore required for accurate projections on a regional scale. Using the complete, latest glacier inventories for the Altai Mountains (Arendt et al. 2014; Nuimura et al. 2015), our projections may have reduced the uncertainties that were unavoidable in previous studies due to incomplete data for the Altai Mountains (e.g. Radić and Hock 2011; Hirabayashi et al. 2013).

Uncertainties associated with GCM projections have been examined in previous studies (Collins et al. 2013; Su et al. 2013), but orographic effects on precipitation and temperature contribute additional uncertainty for mountain regions (Singh and Kumar 1997; Minder et al. 2010). Hence, accurate spatial calculations of high-elevation temperature and precipitation data to force the mass balance model remain a significant challenge in Altai glacier modelling studies. In this study, temperature lapse rates and precipitation gradients are derived from multiple linear regressions, which include the coactions of elevation, longitude and latitude on these parameters. Due to the scarcity of observed meteorological data in high-elevation regions, sensitivity assessments of temperature lapse rate and precipitation gradient, involving running the model with their estimated variable and mean values, are made to assess the influence of different temperature lapse rates and precipitation gradients on model performance. The regional mass loss rates estimated using mean values of temperature lapse rate and precipitation gradient decrease by about 11.1 and 7.3 % with respect to the model run with variable lapse rates and gradients (Zhang et al. 2014), respectively. Here, we also make a similar sensitivity analysis, which involves running the model with an estimated variable and mean temperature lapse rate and precipitation gradient. A comparison of the simulations with variable and constant values of temperature lapse rate and precipitation gradient indicates that the rate of mass loss estimated using their mean values is decreased by about 14 % with respect to the model run with variable lapse rates and gradients (Fig. 4b). As shown in Fig. 4, our model performs well compared to observations from glaciers and simulations from previous studies (Radić and Hock 2011; Wei et al. 2015; Zhang et al. 2014). This implies that consideration of the spatial variability of these parameters substantially reduces model uncertainty and reasonably estimates the forcing data in high-elevation regions.

An ideal treatment of glacier dynamics would couple a physically-based ice dynamics model to a surface mass balance model (e.g. Clarke et al. 2015). It is well recognized that a physically-based treatment of glacier dynamics requires more information about the basal boundary (e.g. ice thickness and basal slip) and surface parameters (e.g. surface velocities and geometry). These required parameters can be obtained through field observations or remote-sensing derivatives, but obtaining these parameters on regional/global scales remains a significate challenge. In addition, without information on the basal boundary, physically-based ice dynamics models typically derive their results solely from surface parameters, leading to an ill-posed inversion with an inherent instability that amplifies short spatial wavelengths and limits model predictions to long spatial wavelengths (Bahr et al. 2015). Therefore, to overcome the scarcity of input parameters, our treatment of glacier dynamics in the Altai Mountains relies on volume-area scaling. This approach represents the accepted method and has been used widely for projecting the future response of the world's glaciers and ice caps to environmental change at different scales (e.g. Radić and Hock 2011; Marzeion et al. 2012; Hirabayashi et al. 2013; Bliss et al. 2014; cf. Bahr et al. 2015). Radić et al. (2007) investigated the application of volume-area scaling for glaciers in different conditions (non-steady and steady states) and found that volume-area scaling agreed well with the results from ice-flow modelling. Furthermore, the scaling approach can capture the feedback between glacier mass balance and changes in glacier hypsometry. Clarke et al. (2015) projected the deglaciation of western Canada by coupling physically-based ice dynamics with a surface mass balance model, and found that the two projections using their method and volume-area scaling for the RCP4.5 and RCP8.5 scenarios are qualitatively similar. Although we cannot assess uncertainty from the scaling approach due to the lack of input parameters required for physically-based ice dynamics models in the Altai Mountains, it can reasonably model changes in glacier area by capturing the feedback between glacier mass balance and changes in glacier hypsometry (Fig. 5).

6 Conclusions

The goal of this study is to provide a quantitative assessment of the variation in surface mass balance and its associated implications by the end of the twenty-first century for the Altai Mountains. The region is projected to experience significant warming in the RCP4.5 and RCP8.5 scenarios throughout the century, with a positive change in precipitation. In response to increasing temperature, the Altai glaciers are predicted to continuously lose mass throughout the century for both RCPs. The mass loss is relatively stable for RCP4.5, while it is accelerated for RCP4.5, in which nearly all glaciers experience dramatic mass loss. While the total glacier area shrinks by 60 ± 15 % for RCP8.5 by 2100 relative to 2005, it decreases by only 26 ± 10 % for RCP4.5. Glacier loss occurs around 2050 for the RCP scenarios with widespread ice disappearance by 2100. Most disappearing glaciers are distributed mainly in the Katun and Chuya ridges and the western part of the Tavan Bogd. All disappearing glaciers in the region are smaller than 5.0 km^2 for RCP4.5, but for RCP8.5, ~7 % of glaciers in the size class of 5.0–10.0 km^2 will also disappear. The rest of the glaciers will survive but in a diminished state.

The meltwater discharge of the region is projected to decrease for the RCPs until mid-century and then to display different trends in the following decades. We project a ~30 % increase in total meltwater discharge in 2091–2100 for RCP8.5 relative to the1986–2005 average, while meltwater discharge for RCP4.5 is projected to decrease by ~39 % relative to the 1986–2005 average. Until 2100, meltwater discharge will not peak for either RCP. In addition, the contribution of glacier loss to sea-level rise over the period 2006–2100 is ~0.0020 mm $year^{-1}$ for RCP4.5, and ~0.0034 mm $year^{-1}$ for RCP8.5. The potential sea-level rise from glacier mass loss in the region is relatively small, but the hydrological implications of the projected mass loss are substantial for the near future, especially for the semi-arid and arid regions of the study area. Although we simplify glacier processes in the projections and this may have affected the model projections, our projections provide an important step forward in understanding the possible future fate of glaciers of different size and the consequent impacts on the water supplies and the regional ecosystem in the study region, where harsh climatic conditions and remoteness hamper ground-based monitoring and result in very poor data coverage.

Acknowledgments This study was supported by MEXT (Japanese Ministry of Education, Culture, Sports, Science and Technology) through the Green Network of Excellence (GRENE) Arctic Climate Change Research Project. We acknowledgement Akiko Sakai of Nagoya University and the RGI consortium for providing glacier inventory data, CMIP5 for GCM scenarios, and WGMS for glacier mass balance data.

References

Arendt A et al (2014) Randolph Glacier Inventory [v4.0]: a dataset of global glacier outlines. Boulder, CO. Digital media
Bahr DB (1997) Width and length scaling of glaciers. J Glaciol 43(145):557–562
Bahr DB, Meier MF, Peckham SD (1997) The physical basis of glacier volume-area scaling. J Geophys Res 102(B9):20355–20362
Bahr DB, Pfeffer WT, Sassolas C, Meier MF (1998) Response time of glaciers as a function of size and mass balance: 1 Theory. J Geophys Res 103(B5):9777–9782. doi:10.1029/98jb00507
Bahr DB, Pfeffer WT, Kaser G (2015) A review of volume-area scaling of glaciers. Rev Geophys 53:95–140. doi:10.1002/2014RG000470
Bliss A, Hock R, Radić V (2014) Global response of glacier runoff to twenty-first century climate change. J Geophys Res 119(4):717–730. doi:10.1002/2013jf002931
Braithwaite RJ, Zhang Y (2000) Sensitivity of mass balance of five Swiss glaciers to temperature changes assessed by tuning a degree-day model. J Glaciol 46(152):7–14. doi:10.3189/172756500781833511
Braithwaite RJ, Zhang Y, Raper SCB (2002) Temperature sensintivity of the mass balance of mountain glaciers and ice caps as a climatiological characteristic. Z Gletsch kd Glazialgeol 38:35–61
Casassa G, López P, Pouyaud B, Escobar F (2009) Detection of changes in glacial run-off in alpine basins: examples from North America, the Alps, central Asia and the Andes. Hydrol Process 23(1):31–41. doi:10.1002/hyp.7194
Clarke GKC, Jarosch AH, Anslow FS, Radić V, Menounos B (2015) Projected deglaciation of western Canada in the twenty-first century. Nat Geosci 8:372–377. doi:10.1038/ngeo2407
Collins M, Knutti R, Arblaster J, Dufresne J-L, Fichefet T, Friedlingstein P, Gao X, Gutowski WJ, Johns T, Krinner G, Shongwe M, Tebaldi C, Weaver AJ, Wehner M (2013) Long-term climate change: projections, commitments and irreversibility. In: Stocker

TF, Qin D, Plattner G-K, Tignor M, Allen SK, Boschung J, Nauels A, Xia Y, Bex V and Midgley PM (eds) Climate change 2013: the physical science basis. Contribution of working group I to the fifth assessment report of the intergovernmental panel on climate change. Cambridge University Press, Cambridge

Cuffey KM, Paterson WSB (2010) The physics of glaciers. Butterworth-Heinemann, Oxford

Dyurgerov MB (2010) Reanalysis of glacier changes: from the IGY to the IPY, 1960–2008. Institute of Arctic and Alpine Research, University of Colorado at Boulder, Boulder

Dyurgerov M, Bring A, Destouni G (2010) Integrated assessment of changes in freshwater inflow to the Arctic Ocean. J Geophys Res 115:D12116. doi:10.1029/2009jd013060

Fang JY, Yoda K (1988) Climate and vegetation in China (I), changes in the altitudinal lapse rate of temperature and distribution of sea level temperature. Ecol Res 3(1):37–51

Graham LP, Andréasson J, Carlsson B (2007) Assessing climate change impacts on hydrology from an ensemble of regional climate models, model scales and linking methods-a case study on the Lule River basin. Clim Change 81(51):293–307. doi:10.1007/s10584-006-9215-2

Hay L, Wilby RL, Leavesley GH (2000) A comparison of delta change and downscaled GCM scenarios for three mountainous basins in the United States. J Am Water Res Assoc 36(2):387–397. doi:10.1111/j.1752-1688.2000.tb04276.x

Hirabayashi Y, Döll P, Kanae S (2010) Global-scale modeling of glacier mass balances for water resources assessments: glacier mass changes between 1948 and 2006. J Hydrol 390:245–256. doi:10.1016/j.jhydrol.2010.07.001

Hirabayashi Y, Zhang Y, Watanabe S, Koirala S, Kanae S (2013) Projection of glacier mass changes under a high-emission climate scenario using the global glacier model HYOGA2. Hydrol Res Lett 7(1):6–11. doi:10.3178/hrl.7.6

Hock R (2003) Temperature index melt modelling in mountain areas. J Hydrol 282:104–115. doi:10.1016/S0022-1694(03)00257-9

Jansson P, Hock R, Schneider T (2003) The concept of glacier storage: a review. J Hydrol 283:116–129. doi:10.1016/S0022-1694(03)00258-0

Kadota T, Gombo D, Kalsan P, Namgur D (2011) Glaciological research in the Mongolian Altai, 2003–2009. Bull Glaciol Res 29:41–50

Kalugin I, Daryin A, Smolyaninova L, Andreev A, Diekmann B, Khlystov O (2007) 800-yr-long records of annual air temperature and precipitation over southern Siberia inferred from Teletskoye Lake sediments. Quat Res 67(3):400–410. doi:10.1016/j.yqres.2007.01.007

Kaser G, Großhauser M, Marzeion B (2010) Contribution potential of glaciers to water availability in different climate regimes. Proc Natl Acad Sci USA 107(47):20223–20227. doi:10.1073/pnas.1008162107

Kitabata H, Sugiura K, Kadota T (2014) Analysis of climate trends in the Altai Mountains between 1988 and 2012. In: Abstract #C41B-0346 presented at 2014 Fall Meeting. AGU, San Francisco. 15–20 Dec 2014

Klinge M, Böhner J, Lehmkuhl F (2003) Climate pattern, snow- and timberlines in the Altai mountains, central Asia. Erdkunde 57(4):296–307. doi:10.3112/erdkunde.2003.04.04

Koirala S, Hirabayashi Y, Mahendran R, Kanae S (2014) Global assessment of agreement among streamflow projections using CMIP5 model outputs. Environ Res Lett 9(6):064017. doi:10.1088/1748-9326/9/6/064017

Li Z, Li K, Wang L (2010) Study on recent glacier changes and their impact on water resources in Xinjiang, North Western China. Quat Sci 30(1):96–106

Li X, Wang L, Chen D, Yang K, Xue B, Sun L (2013) Near-surface air temperature lapse rates in the mainland China during 1962–2011. J Geophys Res 118(14):7505–7515. doi:10.1002/jgrd.50553

Liu Q, Liu S (2015) Response of glacier mass balance to climate change in the Tianshan Mountains during the second half of the twentieth century. Clim Dyn. doi:10.1007/s00382-015-2585-2

Liu Q, Liu S, Zhang Y, Zhang YS (2011) Surface ablation features and recent variation of the lower ablation area of the Hailuogou Glacier, Mt. Gongga. J Glaciol Geocryol 33(2):227–236 **(in Chinese with English abstract)**

Marzeion B, Jarosch AH, Hofer M (2012) Past and future sea-level change from the surface mass balance of glaciers. Cryosphere 6:1295–1322. doi:10.5194/tcd-6-1295-2012

Minder JR, Mote PW, Lundquist JD (2010) Surface temperature lapse rates over complex terrain: lessons from the Cascade Mountains. J Geophys Res 115:D14122. doi:10.1029/2009JD013493

Moss RH, Edmonds JA, Hibbard KA, Manning MR, Rose SK, van Vuuren DP, Carter TR, Emori S, Kainuma M, Kram T, Meehl GA, Mitchell JFB, Nakicenovic N, Riahi K, Smith SJ, Stouffer RJ, Thomson AM, Weyant JP, Wilbanks TJ (2010) The next generation of scenarios for climate change research and assessment. Nature 463:747–756. doi:10.1038/nature08823

Narozhniy Y, Zemtsov V (2011) Current State of the Altai glaciers (Russia) and trends over the period of instrumental observations 1952–2008. Ambio 40(6):575–588. doi:10.1007/s13280-011-0166-0

Nuimura T, Sakai A, Taniguchi K, Nagai H, Lamsal D, Tsutaki S, Kozawa A, Hoshina Y, Takenaka S, Omiya S, Tsunematsu K, Tshering P, Fujita K (2015) The GAMDAM glacier inventory: a quality controlled inventory of Asian glaciers. Cryosphere 9(3):849–864. doi:10.5194/tc-9-849-2015

Oerlemans J, Fortuin JPF (1992) Sensitivity of glaciers and small ice caps to greenhouse warming. Science 258:115–117. doi:10.1126/science.1258.5079.115

Pan CG (2013) Inventory of Mongolian glaciers for the Global Land Ice Measurements from Space (GLIMS) Program. The University of Montana, Montana

Panagiotopoulos F, Shahgedanova M, Hannachi A, Stephenson DB (2005) Observed trends and teleconnections of the Siberian high: a recently declining center of action. J Clim 18(9):1411–1422. doi:10.1175/JCLI3352.1

Pfeffer WT, Arendt AA, Bliss A, Bolch T, Cogley JG, Gardner AS, Hagen J-O, Hock R, Kaser G, Kienholz C, Miles ES, Moholdt G, Mölg N, Paul F, Radic V, Rastner P, Raup BH, Rich J, Sharp MJ (2014) The Randolph Glacier Inventory: a globally complete inventory of glaciers. J Glaciol 60(221):537–652. doi:10.3189/2014JoG13J176

Radić V, Hock R (2011) Regionally differentiated contribution of mountain glaciers and ice caps to future sea-level rise. Nat Geosci 4:91–94. doi:10.1038/ngeo1052

Radić V, Hock R, Oerlemans J (2007) Volume–area scaling vs flowline modelling in glacier volume projections. Ann Glaciol 46:234–240. doi:10.3189/172756407782871288

Radić V, Hock R, Oerlemans J (2008) Analysis of scaling methods in deriving future volume evolutions of valley glaciers. J Glaciol 54(187):601–612. doi:10.3189/002214308786570809

Sakai A, Nuimura T, Fujita K, Takenaka S, Nagai H, Lamsal D (2015) Climate regime of Asian glaciers revealed by GAMDAM glacier inventory. Cryosphere 9(3):865–880. doi:10.5194/tc-9-865-2015

Shahgedanova M, Nosenko G, Khromova T, Muraveyev A (2010) Glacier shrinkage and climatic change in the Russian Altai from the mid-twentieth century: an assessment using remote sensing and PRECIS regional climate model. J Geophys Res 115:D16107. doi:10.1029/2009JD012976

Shi Y, Liu C, Wang Z, Liu S, Ye B (2005) A concise China glacier inventory. Shanghai Science Popularization Press, Shanghai **(in Chinese)**

Singh P, Kumar N (1997) Effect of orography on precipitation in the western Himalayan region. J Hydrol 199(1–2):183–206. doi:10.1016/S0022-1694(96)03222-2

Skamarock WC, Klemp JB (2008) A time-split nonhydrostatic atmospheric model for weather research and forecasting applications. J Comput Phys 227:3465–3485. doi:10.1016/j.jcp.2007.01.037

Skamarock W, Klemp JB, Dudhia J, Gill DO, Barker D, Duda MG, Huang X-Y, Wang W (2008) A Description of the Advanced Research WRF Version 3. NCAR Technical Note NCAR/TN-475 + STR, 10.5065/D68S4MVH. doi:10.5065/D68S4MVH

Sperna Weiland FC, van Beek LPH, Kwadijk JCJ, Bierkens MFP (2010) The ability of a GCM-forced hydrological model to reproduce global discharge variability. Hydrol Earth Syst Sci 14:1595–1621. doi:10.5194/hess-14-1595-2010

Su F, Duan X, Chen D, Hao Z, Cuo L (2013) Evaluation of the global climate models in the CMIP5 over the Tibetan Plateau. J Clim 26:3187–3208. doi:10.1175/JCLI-D-12-00321.1

Sugiura K, Kitabata H and Kadota T (2014) Validation of snow cover simulated by the Weather Research and Forecasting (WRF) model using in situ snow survey data in the Altai Mountains. In: Abstract #C43A-0369 presented at 2014 Fall Meeting. AGU, San Francisco. 15–20 Dec 2014

Surazakov AB, Aizen VB, Aizen EM, Nikitin SA (2007) Glacier changes in the Siberian Altai Mountains, Ob river basin, (1952–2006) estimated with high resolution imagery. Environ Res Lett 2(4):045017. doi:10.1088/1748-9326/2/4/045017

Tachikawa T, Kaku M, Iwasaki A, Gesch D, Oimoen M, Zhang Z, Danielson J, Krieger T, Curtis B, Haase J, Abrams M, Crippen R, Carabajal C (2011) ASTER Global Digital Elevation Model Version 2—Summary of Validation Results. Technical report, NASA Land Processes Distributed Active Archive Center and the Joint Japan-US ASTER Science Team

Taylor KE, Stouffer RJ, Meehl GA (2012) An Overview of CMIP5 and the experiment design. Bull Am Meteorol Soc 93:485–498. doi:10.1175/BAMS-D-11-00094.1

Van Beek LPH (2008) Forcing PCR-GLOBWB with CRU meteorological data. Utrecht University, Utrecht. http://vanbeek.geo.uu.nl/suppinfo/vanbeek2008.pdf

Van Vuuren DP, Edmonds J, Kainuma M, Riahi K, Thomson A, Hibbard K, Hurtt GC, Kram T, Krey V, Lamarque J-F, Masui T, Meinshausen M, Nakicenovic N, Smith SJ, Rose SK (2011) The representative concentration pathways: an overview. Clim Change 109:5–31. doi:10.1007/s10584-011-0148-z

Vaughan DG, Comiso JC, Allison I, Carrasco J, Kaser G, Kwok R, Mote P, Murray T, Paul F, Ren J, Rignot E, Solomina O, Steffen K, Zhang T (2013) Observations: cryosphere. In Stocker TF, Qin D, Plattner G-K, Tignor M, Allen SK, Boschung J, Nauels A, Xia Y, Bex V, Midgley PM (eds) Climate change 2013: the physical science basis. Contribution of working group I to the fifth assessment report of the intergovernmental panel on climate change. Cambridge University Press, Cambridge

Wang XL, Cho H-R (1997) Spatial-temporal structures of trend and oscillatory variabilities of precipitation over Northern Eurasia. J Clim 10:2285–2298

Wei J, Liu S, Xu J, Guo W, Bao W, Shangguan D, Jiang Z (2015) Mass loss from glaciers in the Chinese Altai Mountains between 1959 abd 2008 revealed based on historical maps, SRTM, and ASTER images. J Mt Sci 12:330–343. doi:10.1007/s11629-014-3175-1

WGMS (2014) Fluctuations of Glaciers Database World Glacier Monitoring Service, Zurich, Switzerland. doi:10.5904/wgms-fog-2014-09

Woodward J, Sharp M, Arendt A (1997) The influence of superimposed-ice formation on the sensitivity of glacier mass balance to climate change. Ann Glaciol 24:186–190

Yang W, Yao T, Xu B, Ma L, Wang Z, Wan M (2010) Characteristics of recent temperate glacier fluctuations in the Parlung Zangbo River basin, southeast Tibetan Plateau. Chin Sci Bull 55:2097–2102. doi:10.1007/s11434-010-3214-4

Yao X, Liu S, Guo W, Huai B, Sun M, Xu J (2012) Glacier change of Altay Mountain in China from 1960 to 2009–Based on the Second Glacier Inventory of China. J Nat Resour 27(10):1734–1745 **(in Chinese with English abstract)**

Zhang Y, Liu S, Ding Y (2006) Observed degree-day factors and their spatial variation on glaciers in western China. Ann Glaciol 46:301–306. doi:10.3189/172756406781811952

Zhang Y, Enomoto H, Ohata T, Kitabata H, Kadota T, Hirabayashi Y (2014) Modeling the mass balance of Arctic-Asian glaciers using the WRF data: case study in the Altai Mountains. In: Abstract #C41B-0350 presented at 2014 Fall Meeting. AGU, San Francisco. 15–20 Dec 2014

Zhang Y, Hirabayashi Y, Liu Q, Liu S (2015) Glacier runoff and its impact for a highly glacierized catchment in the south-eastern Tibetan Plateau: past and future trends. J Glaciol 61(228):713–730. doi:10.3189/2015JoG14J188